

An update on Earth's energy balance in light of the latest global observations

Graeme L. Stephens^{1*}, Juilin Li¹, Martin Wild², Carol Anne Clayson³, Norman Loeb⁴, Seiji Kato⁴, Tristan L'Ecuyer⁵, Paul W. Stackhouse Jr⁴, Matthew Lebsock¹ and Timothy Andrews⁶

Climate change is governed by changes to the global energy balance. At the top of the atmosphere, this balance is monitored globally by satellite sensors that provide measurements of energy flowing to and from Earth. By contrast, observations at the surface are limited mostly to land areas. As a result, the global balance of energy fluxes within the atmosphere or at Earth's surface cannot be derived directly from measured fluxes, and is therefore uncertain. This lack of precise knowledge of surface energy fluxes profoundly affects our ability to understand how Earth's climate responds to increasing concentrations of greenhouse gases. In light of compilations of up-to-date surface and satellite data, the surface energy balance needs to be revised. Specifically, the longwave radiation received at the surface is estimated to be significantly larger, by between 10 and 17 Wm⁻², than earlier model-based estimates. Moreover, the latest satellite observations of global precipitation indicate that more precipitation is generated than previously thought. This additional precipitation is sustained by more energy leaving the surface by evaporation — that is, in the form of latent heat flux — and thereby offsets much of the increase in longwave flux to the surface.

Earth's climate is determined by the flows of energy into and out of the planet and to and from Earth's surface. Geographical distributions of these energy flows at the surface are particularly important as they drive ocean circulations, fuel the evaporation of water from Earth's surface and govern the planetary hydrological cycle. Changes to the surface energy balance also ultimately control how this hydrological cycle responds to the small energy imbalances that force climate change¹.

The seminal importance of Earth's energy balance to climate has been understood for more than a century. Although the earliest depictions of the global annual mean energy budget of Earth date to the beginning of the twentieth century^{2,3}, the most significant advance to our understanding of this energy balance occurred after the space age in the 1960s. Among the highlights obtained from early satellite views of Earth was the measurement of Earth's albedo (the ratio of outgoing flux of solar energy to incoming flux from the Sun) at approximately 30% (ref. 4), thus settling a long-standing debate on its magnitude — values ranged between 89% and 29% (ref. 5) before these measurements. The sign and magnitude of the net effect of clouds on the top-of-atmosphere (TOA) fluxes⁶ was also later established with the space-borne observations of the scanning instrument on the Earth Radiation Budget Experiment (ERBE)⁷, which better delineated between clear and cloudy skies. ERBE, and later the Clouds and the Earth's Radiant Energy System (CERES)⁸ and the French Scanner for Radiation Budget⁹, confirmed that the global cloud albedo effect was significantly larger than the greenhouse effect of clouds. Although this was a major advance at the time, determining the influence of clouds on atmospheric and surface fluxes had to wait until the recent satellite measurements of the vertical structure of clouds became available from the A-train¹⁰.

The global annual mean energy balance

The current revised depiction of the global annual mean energy balance for the decade 2000–2010 is provided in Fig. B1. Although the fluxes given are meant to be an average for that decade, the net flux at the TOA (the difference of incoming minus outgoing fluxes) varies on a variety of timescales^{11,12} that include relatively large but episodic changes by volcanic eruptions and a much smaller, more systematic increase associated with increases in ocean heat storage as Earth warms. For the decade considered, the average imbalance is $0.6 = 340.2 - 239.7 - 99.9$ Wm⁻² when these TOA fluxes are constrained to the best estimate ocean heat content (OHC) observations since 2005 (refs 13,14). This small imbalance is over two orders of magnitude smaller than the individual components that define it and smaller than the error of each individual flux. The combined uncertainty on the net TOA flux determined from CERES is ± 4 Wm⁻² (95% confidence) due largely to instrument calibration errors^{12,15}. Thus the sum of current satellite-derived fluxes cannot determine the net TOA radiation imbalance with the accuracy needed to track such small imbalances associated with forced climate change¹¹. Despite this limitation, changes in the CERES net flux have been shown to track the changes in OHC data^{16,17}. This suggests that the intrinsic precision of CERES is able to resolve the small imbalances on interannual timescales^{12,16}, thus providing a basis for constraining the balance of the measured radiation fluxes to time-varying changes in OHC (Supplementary Information). The average annual excess of net TOA radiation constrained by OHC is 0.6 ± 0.4 Wm⁻² (90% confidence) since 2005 when Argo data¹⁴ became available, before which the OHC data are much more uncertain¹⁴. The uncertainty on this estimated imbalance is based on the combination of both the Argo OHC and CERES net flux data¹⁶.

¹Center for Climate Sciences, Jet Propulsion Laboratory, California Institute of Technology, 4800 Oak Grove Drive, Pasadena, California 91109, USA,

²Institute for Atmospheric and Climate Science, ETH Zurich, Universitätsstrasse 16, CH-8092, Zurich, Switzerland, ³Physical Oceanography Department, Woods Hole Oceanographic Institution, 266 Woods Hole Road, Massachusetts 02543, USA, ⁴NASA Langley Research Center, 21 Langley Boulevard, Hampton, Virginia 23681, USA, ⁵Department of Atmospheric Sciences, University of Wisconsin, Madison, Wisconsin 80523, USA, ⁶UK Met Office, FitzRoy Road, Exeter, Devon EX1 3PB, UK. *e-mail: graeme.stephens@jpl.nasa.gov

Box 1 | Updated energy balance

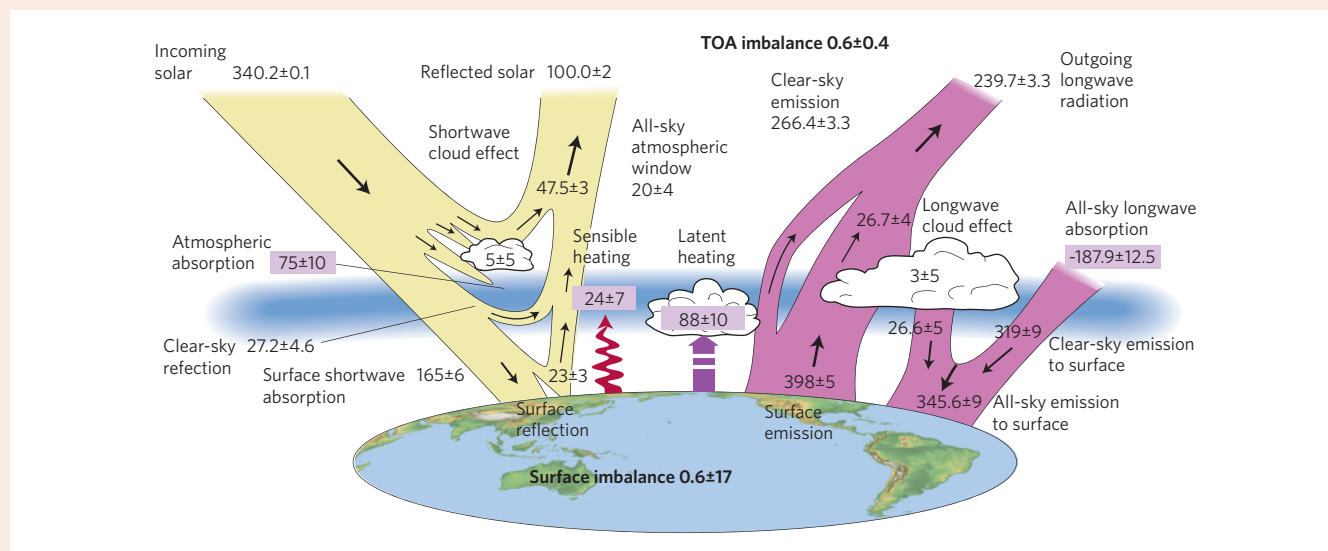


Figure B1 | The global annual mean energy budget of Earth for the approximate period 2000–2010. All fluxes are in Wm^{-2} . Solar fluxes are in yellow and infrared fluxes in pink. The four flux quantities in purple-shaded boxes represent the principal components of the atmospheric energy balance.

A recent compilation of observations (Supplementary Information) provides the depiction of the global annual mean energy balance shown in Fig. B1 for the period 2000–2010. The solar flux entering Earth is the most-accurately monitored of all fluxes through the system⁴⁰ and varies least over time. Fluxes leaving Earth at the TOA are also well documented, although inherently less accurate with an uncertainty of $\pm 4 \text{ Wm}^{-2}$ on the net TOA flux that mostly stems from calibration errors on measurements of the outgoing fluxes^{12,15}. This uncertainty is almost an order of magnitude larger than the imbalance of $0.58 \pm 0.4 \text{ Wm}^{-2}$ inferred from OHC information^{13,14}. The outgoing TOA fluxes presented in Fig. B1 are the TOA CERES fluxes adjusted within the measurement uncertainty to match this OHC inferred imbalance^{15,17}.

A recent review of largely independent global estimates of the surface longwave radiation flux²⁶, also supported by new satellite observations, concludes that this flux most likely falls in the range 342–350 Wm^{-2} , which is larger by 10–17 Wm^{-2} over previous estimates^{41,42} that were mostly based on global weather and climate model outputs that have a known lack of low clouds²⁶. The uncertainty attached to this global annual flux is approximately $\pm 9 \text{ Wm}^{-2}$ (95% confidence), and has also been carefully analysed^{26,43,44} and verified against independent surface observations (Supplementary Information).

Estimating the global net surface solar flux has also been problematic over the years. Five different global estimates of this flux suggest its most likely value is between 162 and 171 Wm^{-2} . The possibility of bias of a few Wm^{-2} cannot be fully discounted, as slightly elevated absorption within the atmosphere by unaccounted gaseous absorption⁴⁵ and an underestimate of the contribution by absorbing aerosol⁴⁶, for example, are factors that could reduce the stated value of the surface flux. A value of $165 \pm 6 \text{ Wm}^{-2}$ is assumed, and the uncertainty attached to this flux (a 90% confidence) is based in part on independent comparison with surface measurements⁴⁷.

The increased downward surface longwave flux dictates that compensating changes to other surface fluxes are required to achieve energy balance. One such adjustment is needed to the latent heat flux. The annual global mean evaporation is balanced

by the annual global precipitation amount, and the common approach to infer the latent heat flux is to use global precipitation measurements⁴⁸. Thus an increase in precipitation implies an increase in evaporation to sustain it and hence a larger flux of energy from the surface associated with this evaporation. There are at least two reasons why past estimates of global latent heat flux deduced from global precipitation should be increased. (1) The remote-sensing methods widely used to estimate precipitation, especially over the vast oceans, have documented biases that imply that the amount of precipitation is underestimated^{49–52}. New global precipitation information from the CloudSat radar suggests that precipitation has been underestimated by approximately 10% over tropical ocean regions⁴⁹ and by even larger fractions over mid-latitude oceans^{51–53}. (2) The total contribution from snowfall to the global precipitation is also not precisely known and has been excluded from previous global latent heat flux estimates. Based on new estimates of global snowfall⁵⁴, we estimate the contribution to the total global latent heating is approximately 4 Wm^{-2} (Supplementary Information). For these reasons, the value of latent heat flux stated in Fig. B1 has been increased by 4 Wm^{-2} over the Global Precipitation Climatology Project⁴⁹ estimate of 76 Wm^{-2} and then increased by 10% (8 Wm^{-2}). The uncertainty on annual oceanic mean precipitation lies between approximately $\pm 10\%$ and $\pm 20\%$ (refs 51,56). The quoted uncertainty on the evaporation ($\pm 10 \text{ Wm}^{-2}$) derives from our very sketchy understanding of the uncertainty in global precipitation.

The quoted value of the sensible heat flux is a combination of the land⁵⁷ and ocean (C. A. Clayson, J. B. Roberts and A. S. Bogdanoff, manuscript in preparation) sensible heat fluxes (Supplementary Information) with a simple weighting based on land/ocean surface area. The flux value of 24 Wm^{-2} is also larger than previously assumed^{41,42} and remains highly uncertain, as exemplified by the range of 14–34 Wm^{-2} that results from different land flux estimates⁵⁷. No definitive measure of the uncertainty of this flux exists and the uncertainty range given merely reflects a judgement on where the value most likely lies. As yet, there are no estimates of the sensible heat fluxes over the polar regions of sea ice and the global values given in Fig. B1 exclude these contributions.

The surface radiative fluxes summarized in Fig. B1 are an average of five different estimates that use mixtures of global satellite data, surface measurements and atmospheric-state information from global weather analysis products (Supplementary Information). Measurements of solar flux incident at Earth's surface, like the TOA fluxes, reveal flux variations on decadal timescales¹⁸ arising from increasing and decreasing aerosols, decadal variability in cloudiness and the effects of volcanic eruptions¹⁹. The effects of large volcanic eruptions, such as the Pinatubo eruption in 1991, reduce the surface shortwave flux received at the surface by up to 5 Wm^{-2} (refs 11,12) over 1–2 years, with suggestions that these changes reduce precipitation over land and river runoff²⁰.

Although much of the discussion on climate change has focused on the TOA energy balance, the importance and relevance of the energy balance at the surface has gained recent emphasis^{1,21}, in part because changes to surface energy control the global precipitation response to climate forcings^{1,22,23}. The connection between the energy balance and the global hydrological cycle follows from a closer look at the surface energy balance summarized more conveniently in Fig. B1. Evaporation at the surface ($88 \pm 10 \text{ Wm}^{-2}$) is the main process that consumes most of the net surplus solar radiant energy ($165 \pm 6 \text{ Wm}^{-2}$) followed by net emission from the surface ($398 - 345 = 53 \pm 9 \text{ Wm}^{-2}$) and then sensible heating ($24 \pm 7 \text{ Wm}^{-2}$). The heat transferred to the atmosphere through the turbulent process of latent and sensible heating balances the net atmospheric loss of radiant energy ($-112 \pm 15 \text{ Wm}^{-2} = 74 + 398 - 239 - 345$; Fig. B1), given that the annual mean heat storage of the atmosphere is negligible. As the latent heat flux to first order balances the loss of energy from the atmosphere by radiation processes, any long-term alterations to this radiation heat loss can be expected to induce long-term changes to the global evaporation and thus the global water cycle^{23,24}.

The effect of clouds on the TOA fluxes has also been well documented since the time of ERBE measurements. The so-called albedo effect of clouds enhances the reflected solar flux by $47.5 \pm 3 \text{ Wm}^{-2}$, whereas clouds reduce the outgoing longwave flux relative to clear skies by approximately $26.4 \pm 4 \text{ Wm}^{-2}$ (a measure of their greenhouse effect). This gives a net loss of radiation from Earth by clouds of $21.1 \pm 5 \text{ Wm}^{-2}$, mostly by reflection of sunlight from clouds in the mid-latitude summer hemisphere⁷. What is new about Fig. B1 is that it also includes results drawn from the new satellite observations of CloudSat and CALIPSO, which provide the tools to quantify the effects of clouds on both the surface and atmospheric energy balance²⁵ in a more definitive way. The enabling information is the vertical profile of clouds, which provides the cloud-base-height information needed to determine the enhanced emission by clouds to the surface more directly²⁶ ($28 \pm 9 \text{ Wm}^{-2}$), and thus has removed a lingering source of uncertainty in estimating the surface longwave flux. The cloud profile information also provides the basis for estimating the atmospheric absorption of radiation by clouds ($8 \pm 7 \text{ Wm}^{-2}$)²⁷. The influence of clouds on both the outgoing TOA and downward surface longwave fluxes predominantly occurs in what is referred to as the 'window region' of the infrared absorption spectrum. This window is a spectral region where the atmosphere is more transparent than in adjacent stronger absorbing regions of the spectrum. This window is not completely transparent and the flux that passes through has contributions from the atmosphere of varying amounts — more in tropical regions and much less in higher, drier latitudes²⁸. Recent calculations²⁹ suggest that the contribution to the global mean clear-sky TOA flux by emissions escaping through this window region is 66 Wm^{-2} , reduced to $20 \pm 4 \text{ Wm}^{-2}$ for the all-sky conditions owing to absorption of this emitted radiation by clouds.

The energy balance and climate change

A comparison between the fluxes summarized in Fig. 1 and

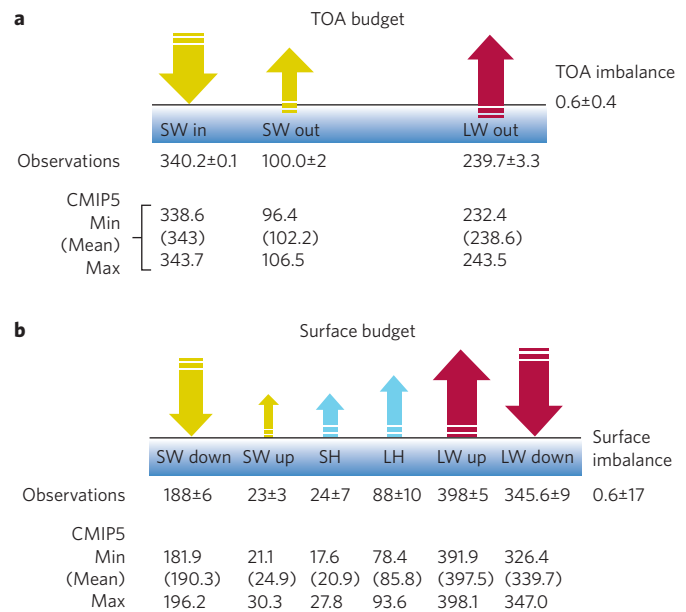


Figure 1 | Surface energy balance. Observed and climate model deduced energy fluxes (all in Wm^{-2}) in and out of the TOA (**a**) and at the surface (**b**). The observed fluxes (containing error estimates) are taken from Fig. B1 and the climate model fluxes are from simulations archived under the World Climate Research Programme's Coupled Model Intercomparison Project phase 5 (CMIP5) twentieth-century experiments. The fluxes from a 16-model ensemble are summarized in terms of the range in model values (maximum and minimum fluxes) with the ensemble mean fluxes given in parenthesis. 'SW in' and 'SW out' refer to the incoming and outgoing (reflected) solar fluxes at the TOA and 'LW out' is the outgoing longwave radiation. Similarly 'SW down' and 'SW up' refer to downward and upward (reflected) solar fluxes at the surface, and 'LW up' and 'LW down' refer to the upward emitted flux of longwave radiation from the surface and the downward longwave flux emitted from the atmosphere to the surface, respectively. SH and LH refer to latent and sensible heat fluxes.

fluxes derived from climate models (Supplementary Information) provides both an assessment of the performance of these models in simulating the current energy balance of the climate system and a useful basis for understanding the projected changes to the energy balance associated with climate change (Fig. 2). Models are commonly tuned to the TOA, so direct comparison of TOA fluxes provides little insight into model performance. As the surface solar flux is also correlated to the TOA reflected solar flux³⁰, that flux is also not entirely free of 'tuning' effects, so a direct comparison with estimated surface solar flux also has to be interpreted cautiously. The remaining surface fluxes, however, are completely uncoupled from the TOA fluxes³¹ and comparison with observations reveals important insights about model energy balances. The model fluxes given in Fig. 1 are expressed as a multi-model average and a range indicated by maxima and minima fluxes of the model ensemble. The inter-model global mean fluxes lie within the uncertainty of the observed values, and the global mean downward longwave surface fluxes taken from climate models generally lie at the low end of the uncertainty range of the estimated fluxes as noted in other studies^{26,32}. It is also notable that the model latent heat fluxes are closer to the new revised flux (Box 1). Although model and observations broadly agree in the global mean, important regional biases exist in the modelled energy budgets that are not conveyed in global mean statistics³³.

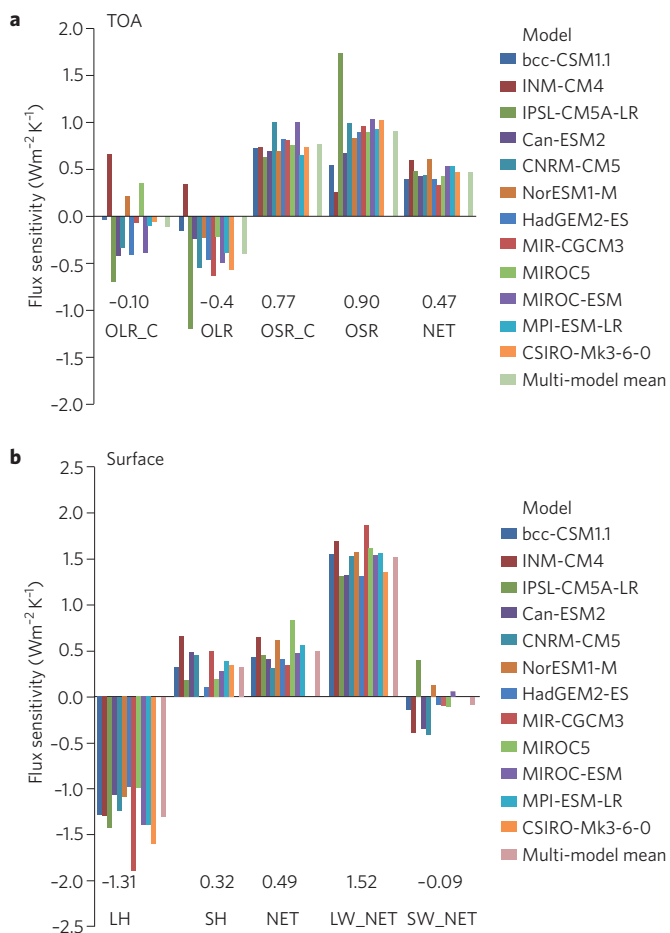


Figure 2 | The change in energy fluxes expressed as flux sensitivities (Wm⁻² K⁻¹) due to a warming climate. TOA flux (a) and surface flux (b) sensitivities derived from a 12-model ensemble from the Coupled Model Intercomparison Project phase 5 150-year model simulations forced by a 1% per year increase in carbon dioxide. Also included are multi-model mean values (also in Wm⁻² K⁻¹). All-sky short- and longwave fluxes refer to the fluxes from Earth that combine both clear and cloudy skies. The TOA flux sensitivities include the clear-sky OLR (OLR_C), the all-sky OLR (OLR), the clear-sky outgoing solar radiation (OSR_C) and the all-sky outgoing solar radiation (OSR). The NET TOA sensitivity is the sum of the short- and longwave all-sky flux sensitivities at the TOA with positive values implying a gain of heat within the system. The NET at the surface is the combination of the net (downward minus upward) all-sky short- (SW_NET) and longwave (LW_NET) fluxes plus the sensitivities of the sensible (SH) and latent heat (LH) fluxes. A positive value of surface NET also implies heat gained by the surface.

The magnitude of change associated with a warming forced by increased concentrations of carbon dioxide can also be examined using climate models that are forced with a prescribed change in carbon dioxide. Small perturbations to the global annual mean energy fluxes induced by the 1% per year increase in carbon dioxide are approximately linear with respect to the global mean change in surface air temperature (Supplementary Information), and this linear sensitivity offers a convenient framework for comparing models of very different overall climate sensitivity. The average of 12 different climate models indicates that a global warming induced by carbon dioxide increases is forced by a small TOA energy imbalance of +0.46 Wm⁻² K⁻¹ (Fig. 2a). This imbalance is formed by generally opposing increases in radiation emitted to space (-0.39 Wm⁻² K⁻¹) and decreases in reflected solar flux

(0.86 Wm⁻² K⁻¹), mostly apparent in the clear-sky flux changes (0.77 Wm⁻² K⁻¹). The decrease in reflected solar flux is approximately equally divided between reduced reflection from decreased snow/ice cover and by reduced reflection resulting from increased absorption of solar radiation by water vapour. Models are much less in agreement, however, about how the longwave fluxes change and how clouds affect both the TOA short- and longwave fluxes as evident in comparison of the all-sky and clear-sky longwave fluxes (Fig. 2a).

The surface warming of the models is sustained by an equivalent small imbalance of the surface energy budget of +0.45 Wm⁻² K⁻¹. Although this imbalance closely matches the TOA imbalance in value, it is mainly constructed from changes to three fluxes that dwarf the changes in the other surface fluxes. The change to the downward longwave flux at the surface is approximately 7 Wm⁻² K⁻¹, mostly occurring as a clear-sky flux change^{23,26} (Fig. 2b). This is the largest change of all fluxes in Earth's climate system and is partially offset by the increase in upward longwave flux resulting from the surface warming, resulting in a net (downward minus upward) longwave flux increase of +1.52 Wm⁻² K⁻¹ (inter-model mean). This increased net flux to the surface is the driving force of the surface warming and is largely balanced by the increased flux associated with evaporation (-1.29 Wm⁻² K⁻¹). Thus an important, distinguishing difference emerges between both the energy balance of the mean climate state (Fig. B1), and a perturbed climate forced by greenhouse-gas increases. The source of evaporation and its change in the mean climate state is driven by the amount of solar radiation at the surface and changes to it, whereas the change in evaporation in a greenhouse-gas-forced climate change is driven mostly by surface longwave flux changes (Fig. 2b)²³. Changes to the surface net solar flux can also fuel both changes in evaporation and changes to surface temperature, and thus the emitted longwave flux from the surface. There is, however, little consensus across the models presented in Fig. 2b as to how much change occurs in the net surface solar flux in a warming climate. As with the TOA solar fluxes, this disagreement in both magnitude and sign mostly occurs with cloudy-sky fluxes, and reflects the range in shortwave cloud feedbacks that operate in models³⁴.

The challenge ahead

Satellite observations combined with other data (Box 1) now convincingly support previous observation-based estimates of the surface downward longwave flux. The revised estimates of these fluxes range between 342 and 350 Wm⁻², and are between 10 and 17 Wm⁻² larger than past estimates that have relied primarily on global models. Recent satellite observations of global precipitation also indicate that Earth produces more precipitation than previously accounted for. Thus the flux of latent heat leaving the surface that sustains this increased precipitation is also larger than has been assumed. This elevated flux offsets much of the revised larger longwave flux to the surface.

The net energy balance is the sum of individual fluxes. The current uncertainty in this net surface energy balance is large, and amounts to approximately 17 Wm⁻². This uncertainty is an order of magnitude larger than the changes to the net surface fluxes associated with increasing greenhouse gases in the atmosphere (Fig. 2b). The uncertainty is also approximately an order of magnitude larger than the current estimates of the net surface energy imbalance of 0.6 ± 0.4 Wm⁻² inferred from the rise in OHC^{13,14}. The uncertainty in the TOA net energy fluxes, although smaller, is also much larger than the imbalance inferred from OHC. The variations of these fluxes on interannual timescales¹², however, closely follow variations in changes to OHC over time^{13,14,16}. This link makes it possible at least to anchor the TOA net fluxes to these changes in OHC and place a tighter constraint on the TOA energy balance.

No attempt has yet been made to examine the extent that changes in the surface energy balance over time similarly track changes in OHC as would be expected.

Surface energy budgets, like the one reported here, are at present constructed from information about individual fluxes created independently by different groups. Inconsistencies typically arise when these different components are brought together to form a balance. Because previous energy-balance studies have generally failed to address the uncertainties in these flux components, subsequent adjustments to surface fluxes to achieve balance have little merit. As well as information on OHC, other sources of typically unused information exist about different combinations of these fluxes that could be better exploited. For example, information about the atmospheric water balance from measurements of water vapour and winds provides a way of constraining regional differences between precipitation and evaporation^{35,36}, as do ocean salinity measurements³⁷. The measurement of gravity fluctuations from the Gravity Recovery and Climate Experiment mission³⁸ also provide information about accumulation of snow over vast ice masses and an alternative way of constraining the contribution of snow to the latent heat flux³⁹ (Supplementary Information), among other uses. To produce a more accurate depiction of the energy balance of Earth, all such available resources need to be integrated, together with more sophisticated ways of assimilating these data and appropriate constraints. Essential observations such as precipitation, TOA radiative fluxes, ocean surface winds, and clouds have to be sustained if progress is to continue. But even with these steps in place, the precision needed to monitor the changes in fluxes associated with forced climate change remains a significant challenge.

Received 8 November 2011; accepted 13 August 2012;
published online 23 September 2012

References

- Andrews, T., Forster, P. M. & Gregory, J. M. A surface energy perspective on climate change. *J. Clim.* **22**, 2557–2570 (2009).
- Abbot, C. G. & Fowle, F. E. Radiation and terrestrial temperature. *Ann. Astrophys. Obs. Smithsonian Inst.* **2**, 125–224 (1908).
- Dines, W. H. The heat balance of the atmosphere. *Q. J. R. Meteorol. Soc.* **43**, 151–158 (1917).
- Vonder Haar, T. H. & Suomi, V. Measurements of the Earth's radiation budget from satellites during a 5 year period. I. Extended time and space means. *J. Atmos. Sci.* **28**, 305–314 (1971).
- Hunt, G. E., Kandel, R. & Mecherikunnel, A. T. A history of pre-satellite investigations of the Earth's radiation budget. *Rev. Geophys.* **24**, 351–356 (1986).
- Stephens, G. L., Campbell, G. & Vonder Haar, T. Earth radiation budgets. *J. Geophys. Res.* **86**, 9739–9760 (1981).
- Harrison, E. F. *et al.* Seasonal variation of cloud radiative forcing derived from the Earth Radiation Budget Experiment. *J. Geophys. Res.* **95**, 18687–18703 (1990).
- Wielicki, B. A. *et al.* Clouds and the Earth's Radiant Energy System (CERES): An Earth observing system experiment. *Bull. Am. Meteorol. Soc.* **77**, 853–868 (1996).
- Kandel, R. *et al.* The ScaRaB Earth radiation budget dataset. *Bull. Am. Meteorol. Soc.* **79**, 765–783 (1998).
- Stephens, G. L. *et al.* The CloudSat mission and the A-train. *Bull. Am. Meteorol. Soc.* **83**, 1771–1790 (2002).
- Hansen, J. *et al.* Earth's energy imbalance: Confirmation and implications. *Science* **308**, 1431–1435 (2005).
- Harries, J. E. & Belotti, C. On the variability of the global net radiative energy balance of the nonequilibrium Earth. *J. Clim.* **23**, 1277–1290 (2010).
- Lyman, J. M. *et al.* Robust warming of the global upper ocean. *Nature* **465**, 334–337 (2010).
- Willis, J. K., Lyman, J. M., Johnson, G. C. & Gilson, J. *In situ* data biases and recent ocean heat content variability. *J. Atmos. Ocean. Technol.* **26**, 846–852 (2009).
- Loeb, N. *et al.* Toward optimal closure of the Earth's top-of-atmosphere radiation budget. *J. Clim.* **22**, 748–766 (2009).
- Loeb, N. *et al.* Heating of Earth's climate system continues despite lack of surface warming in past decade. *Nature Geosci.* **5**, 110–113 (2012).
- Wong, T. *et al.* Reexamination of the observed decadal variability of the Earth radiation budget using altitude corrected ERBE/ERBS non scanner WFOV data. *J. Clim.* **19**, 4028–4040 (2006).
- Wild, M. J., Grieser, J. & Schar, C. Combined surface solar brightening and increasing greenhouse effect support recent intensification of the global land-based hydrological cycle. *Geophys. Res. Lett.* **35**, L17706 (2008).
- Streets, D. G. *et al.* Discerning human and natural signatures in regional aerosol trends. *J. Geophys. Res.* **114**, D00D18 (2009).
- Trenberth, K. E. & Dai, A. Effects of Mount Pinatubo volcanic eruption on the hydrological cycle as an analog of geoengineering. *Geophys. Res. Lett.* **34**, L15702 (2007).
- National Research Council *Radiative Forcing of Climate Change* (National Academies Press, 2005).
- Allen, M. R. & Ingram, W. J. Constraints on future changes in climate and the hydrologic cycle. *Nature* **419**, 224–232 (2002).
- Stephens, G. L. & Ellis, T. D. Controls of global-mean precipitation increases in global warming GCM experiments. *J. Clim.* **21**, 6141–6155 (2008).
- Stephens, G. L. & Hu, Y. Are climate-related changes to the character of global precipitation predictable? *Environ. Res. Lett.* **5**, 025209 (2010).
- Stephens, G. L. *et al.* The CloudSat mission: Performance and early science after the first year of operation. *J. Geophys. Res.* **113**, D00A18 (2008).
- Stephens, G. L. *et al.* The global character of the flux of downward longwave radiation. *J. Clim.* **25**, 557–571 (2012).
- L'Ecuyer, T. S., Wood, N. B., Haladay, T., Stephens, G. L. & Stackhouse, P. W. Jr Impact of clouds on the atmospheric heating based on the R04 CloudSat fluxes and heating rates data set. *J. Geophys. Res.* **113**, D00A15 (2008).
- Clough, S. A., Iacono, M. J. & Moncet, J.-L. Line-by-line calculations of atmospheric fluxes and cooling rates: Application to water vapor. *J. Geophys. Res.* **97**, 761–785 (1992).
- Costa, S. M. S. & Shine, K. P. Outgoing longwave radiation due to directly transmitted surface emission. *J. Atmos. Sci.* **69**, 1865–1870 (2012).
- Li, Z. & Leighton, H. G. Global climatologies of solar radiation budgets at the surface and in the atmosphere from 5 years of ERBE data. *J. Geophys. Res.* **98**, 4919–4930 (1993).
- Stephens, G. L. & Webster, P. J. Cloud decoupling of the surface and planetary radiative budgets. *J. Atmos. Sci.* **41**, 681–686 (1984).
- Wild, M. Short-wave and long-wave surface radiation budgets in GCMs: A review based on the IPCC-AR4/CMIP3 models. *Tellus A* **60**, 932–945 (2008).
- Trenberth, K. E. & Fasullo, J. T. Global warming due to increasing absorbed solar radiation. *Geophys. Res. Lett.* **36**, L07706 (2009).
- Bony, S. *et al.* How well do we understand and evaluate climate change feedback processes? *J. Clim.* **19**, 3445–3482 (2006).
- Wong, S. *et al.* Closing the global water budget with AIRS water vapor, MERRA winds, and evaporation, and TRMM precipitation. *J. Clim.* **24**, 6307–6321 (2011).
- Liu, W. T., Xie, X., Tang, W. & Zlotnicki, V. Space-based observations of oceanic influence on the annual variation of South American water balance. *Geophys. Res. Lett.* **33**, L08710 (2006).
- Durack, P. J. & Wijffels, S. E. Fifty-year trends in global ocean salinities and their relationship to broad-214 scale warming. *J. Clim.* **23**, 4342–4361 (2010).
- Tapley, B. D., Bettadpur, S., Ries, J. C., Thompson, P. F. & Watkins, M. GRACE measurements of mass variability in the Earth system. *Science* **305**, 503–505 (2004).
- Swenson, S. Assessing high-latitude winter precipitation from global precipitation analyses using GRACE. *J. Hydrometeorol.* **11**, 405–420 (2010).
- Kopp, G. & Lean, J. L. A new, lower value of total solar irradiance: Evidence and climate significance. *Geophys. Res. Lett.* **38**, L01706 (2011).
- Kiehl, J. T. & Trenberth, K. E. Earth's annual global mean energy budget. *Bull. Am. Meteorol. Soc.* **78**, 197–208 (1997).
- Trenberth, K. E., Fasullo, J. T. & Kiehl, J. Earth's global energy budget. *Bull. Am. Meteorol. Soc.* **90**, 311–324 (2009).
- Zhang, Y.-C., Rossow, W. B., Laci, A. A., Oinas, V. & Mishchenko, M. I. Calculation of radiative fluxes from the surface to top of atmosphere based on ISCCP and other global data sets: Refinements of the radiative transfer model and the input data. *J. Geophys. Res.* **109**, D19105 (2004).
- Kato, S. *et al.* Computation of top-of-atmosphere and surface irradiance with CALIPSO, CloudSat, and MODIS-derived cloud and aerosol properties. *J. Geophys. Res.* **116**, D19209 (2011).
- Ptashnik, I. V., Shine, K. P. & Vigasin, A. A. Water vapour self-continuum and water dimers: 1. Analysis of recent work. *J. Quant. Spectrosc. Radiat. Transf.* **112**, 1286–1303 (2011).
- Ramanathan, V., Crutzen, P. J., Kiehl, J. T. & Rosenfeld, D. Aerosols, climate, and the hydrological cycle. *Science* **294**, 2119–2124 (2001).
- Stackhouse, P. W. Jr *et al.* The NASA/GEWEX surface radiation budget release 3.0, 24.5-year dataset. *GEWEX News* **21**, 10–12 (February 2011).
- Trenberth, K. E., Smith, L., Qian, T., Dai, A. & Fasullo, J. Estimates of the global water budget and its annual cycle using observational and model data. *J. Hydrometeorol.* **8**, 758–769 (2007).

49. Berg, W., L'Ecuyer, T. & Haynes, J. M. The distribution of rainfall over oceans from space-borne radars. *J. Appl. Meteorol. Climatol.* **49**, 535–543 (2010).
50. Ellis, T. D., L'Ecuyer, T. S., Haynes, J. M. & Stephens, G. L. How often does it rain over the global oceans? The perspective from CloudSat. *Geophys. Res. Lett.* **36**, L03815 (2009).
51. Haynes, J. M. *et al.* Rainfall retrieval over the ocean with spaceborne W-band radar. *J. Geophys. Res.* **114**, D00A22 (2009).
52. Dai, A., Lin, X. & Hsu, K-L. The frequency, intensity, and diurnal cycle of precipitation in surface and satellite observations over low- and mid-latitudes. *Clim. Dynam.* **29**, 727–744 (2007).
53. Petty, G. W. An inter-comparison of oceanic precipitation frequencies from 10 special sensor microwave/imager rain rate algorithms and shipboard present weather reports. *J. Geophys. Res.* **102**, 1757–1777 (1997).
54. Liu, G. Deriving snow cloud characteristics from CloudSat observations. *J. Geophys. Res.* **113**, D00A09 (2008).
55. Adler, R. F. *et al.* The version 2 global precipitation climatology project (GPCP) monthly precipitation analysis (1979–present). *J. Hydrometeorol.* **4**, 1147–1167 (2003).
56. L'Ecuyer, T. S. & Stephens, G. L. An uncertainty model for Bayesian Monte Carlo retrieval algorithms: Application to the TRMM observing system. *Q. J. R. Meteorol. Soc.* **128**, 1713–1737 (2002).
57. Jimenez, C. *et al.* Global intercomparison of 12 land surface heat flux estimates. *J. Geophys. Res.* **116**, D02102 (2011).

Additional information

Supplementary information accompanies this paper on www.nature.com/naturegeoscience. Reprints and permissions information is available online at www.nature.com/reprints. Correspondence and requests for materials should be addressed to G.L.S.